

Magneto-optical polarization rotation in a ladder-type atomic system for tunable offset locking

Michał Parniak,^{1, a)} Adam Leszczyński,¹ and Wojciech Wasilewski¹

Institute of Experimental Physics, Faculty of Physics, University of Warsaw, Pasteura 5, 02-093 Warsaw, Poland

We demonstrate an easily tunable locking scheme for stabilizing frequency-sum of two lasers on a two-photon ladder transition based on polarization rotation in warm rubidium vapors induced by magnetic field and circularly polarized drive field. Unprecedented tunability of the two-photon offset frequency is due to strong splitting and shifting of magnetic states in external field. In our experimental setup we achieve two-photon detuning of up to 700 MHz.

Two-photon transitions allowing excitation to higher excited states are one of the most promising candidates for engineering light-atoms interactions. They facilitate control of Rydberg atoms¹ or ground-state coherence², a two-color magneto-optical trap^{3,4}, and a variety of other nonlinear wave-mixing processes^{5–8}.

In numerous scenarios detuning the lasers from two-photon resonance by a stable and well-controlled frequency offset is required. To obtain a steep locking signal, one may modulate the absorption⁹, transmission¹⁰ or electromagnetically-induced transparency signals^{11,12}, or use modulation transfer spectroscopy¹³. Alternatively, one can use Doppler-free polarization spectroscopy to obtain the locking signal without modulation^{14–17}. Nevertheless, tunability of the two-photon detuning requires additional modulation at the offset frequency¹⁸.

In this Letter we present a modulation-free, easily tunable scheme for frequency-sum stabilization of two lasers on a ladder transition. By changing the magnetic field we are able to tune the dispersively shaped locking signal around the two-photon resonance. The underlying principle is the polarization rotation of probe light induced by circular polarization of drive field and external magnetic field. Varying the magnetic field within a small range of ± 60 G offers unprecedented tunability of over 1 GHz. Magnetic field has previously been used in the two-photon variation of commonly employed dichroic atomic vapor laser lock setup, but exclusively to obtain the Doppler-free steep signal itself¹⁹. The setup did not offer tunability of the two-photon offset frequency. Tuning capability of magnetic field has only been used so far in absorptive²⁰ or Faraday anomalous dispersion filters²¹ based on atomic vapors.

Figure 1 shows atomic levels involved in the locking scheme. Linearly polarized probe field \mathbf{A}_1 at 780 nm is far-detuned from the single-photon transition $5S_{1/2}$, $F = 1 \rightarrow 5P_{3/2}$ of ^{87}Rb . Respective detuning Δ is larger than both the hyperfine splitting of $5P_{3/2}$ state and the Doppler FWHM linewidth of approx. 635 MHz. Circularly polarized drive field \mathbf{A}_2 at 776 nm is detuned from the $5P_{3/2} \rightarrow 5D_{5/2}$ transition by $\delta - \Delta$, so the two lasers

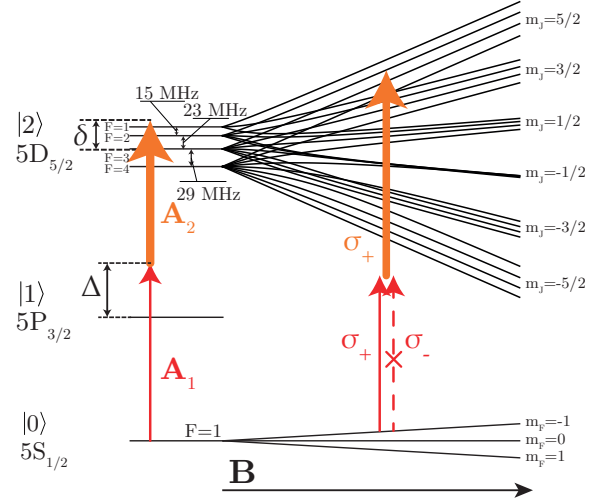


Figure 1. Atomic structure of ^{87}Rb used in the experiment with a diagram of levels splitting of the ground and highest excited states in magnetic field of up to 50 G. While the ground states remains well within the Zeeman regime, the $5D_{5/2}$ manifold reaches the hyperfine Paschen-Back regime, since its hyperfine dipole constant $A_{5D_{5/2}} = -7.44$ MHz²² is quite small. Circularly polarized drive field creates imbalance in susceptibilities for two circular polarizations of the probe field, giving rise to circular birefringence and in turn polarization rotation.

have combined nonzero two-photon detuning δ from the line centroid. Counter-propagating configuration results in nearly perfect cancellation of Doppler broadening for the two-photon transition. Magnetic states are split in static magnetic field $\mathbf{B} = B_z \mathbf{e}_z$ (along the propagation axis z of probe light).

Polarization rotation occurs due to birefringence induced by circularly polarized drive field and applied external magnetic field. Magnetic field also enables tuning, as it shifts atomic levels. In turn, the locking signal at different frequencies is obtained.

To describe the locking signal lineshapes we first adopt the model of an isolated three level atom in ladder configuration. The atom is probed by field of amplitude \mathbf{A}_1 and driven by field of amplitude \mathbf{A}_2 . The susceptibility for the probe field corresponding to the steady-state solution of Maxwell-Bloch equations reads:

^{a)} Electronic mail: michal.parniak@fuw.edu.pl

$$\chi = -\frac{N}{\hbar\epsilon_0} \frac{|\mathbf{d}_{01}|^2}{\Delta + i\Gamma/2 - |\Omega_2|^2/4(\delta + i\gamma/2)}, \quad (1)$$

where N is the atom number density and $\Omega_2 = \mathbf{A}_2 \cdot \mathbf{d}_{12}/\hbar$ is the Rabi frequency. Dipole moments of respective transitions are given by \mathbf{d}_{01} and \mathbf{d}_{12} and relaxation rates of states $|1\rangle$ and $|2\rangle$ are given by $\Gamma = 2\pi \times 6.06$ MHz²³ and $\gamma = 2\pi \times 0.66$ MHz²⁴, respectively. For the single-photon detuning $\Delta \gg \Omega_2, \Gamma$, we obtain an expression with two terms:

$$\chi = -\frac{N}{\hbar\epsilon_0} \left(\frac{|\mathbf{d}_{01}|^2|\mathbf{d}_{12}|^2|\mathbf{A}_2|^2}{4\hbar^2\Delta^2(\delta + i\gamma/2)} + \frac{|\mathbf{d}_{01}|^2}{\Delta} \right). \quad (2)$$

The first term is resonant and dominates around $\delta = 0$. The second, linear dispersion term is very slowly-varying. Consequently, for our considerations we may drop the latter and focus on the first, two-photon term.

To calculate the susceptibility for the atom having a rich hyperfine structure, we sum over all possible sublevels $|n, \alpha\rangle$ (shifted in frequency by $\omega_{n,\alpha}$) of each manifold n , thus taking into account all possible two-photon transitions from $|0, \alpha\rangle$ to $|2, \alpha'\rangle$:

$$\chi_{q_1, q_2} = -\frac{N}{4\hbar^3\epsilon_0} \sum_{\alpha, \alpha', \alpha''} \frac{|\langle 2, \alpha'' | \hat{d}_{q_2} | 1, \alpha' \rangle \langle 1, \alpha' | \hat{d}_{q_1} | 0, \alpha \rangle|^2 |\mathbf{A}_2|^2}{(\Delta - \omega_{0,\alpha} + \omega_{1,\alpha'})^2 (\delta - \omega_{0,\alpha} + \omega_{2,\alpha''} + i\gamma/2)}, \quad (3)$$

where $\omega_{n,\alpha}$ is the shift of a particular sublevel $|n, \alpha\rangle$ from the centroid, \hat{d}_q is the dipole moment operator and light polarizations of fields \mathbf{A}_1 and \mathbf{A}_2 are given by q_1 and q_2 . Since the single-photon detuning Δ is far off-resonant we may neglect hyperfine and magnetic splitting of the intermediate state and drop the $\omega_{1,\alpha'}$ term in the above expression. This simplifies the summation, since now the summation over intermediate states indexed by α' may be done separately. To find the dipole matrix elements, we first solve the eigenproblem for the Hamiltonian in $|n, m_I, m_J\rangle$ basis for each manifold n :

$$\hat{H}_n = \mu_B g_{n,J} B_z \hat{J}_{n,z} + A_n \hat{\mathbf{I}}_n \cdot \hat{\mathbf{J}}_n, \quad (4)$$

where μ_B is the Bohr magneton, $g_{n,J}$ is the Landé factor, A_n is the hyperfine dipole coupling constant and $\hat{\mathbf{I}}_n$ and $\hat{\mathbf{J}}_n$ are nuclear and electronic angular momentum operators, respectively, for hyperfine manifold n . We find decomposition of $|n, \alpha\rangle$ in $|n, m_I, m_J\rangle$ basis and respective energy shifts of levels $\hbar\omega_{n,\alpha}$. Using this decomposition we are able to transform the dipole matrix to Hamiltonian eigenbasis.

Finally, transmitted light intensities are calculated in circular polarization basis. Here, we give our result for

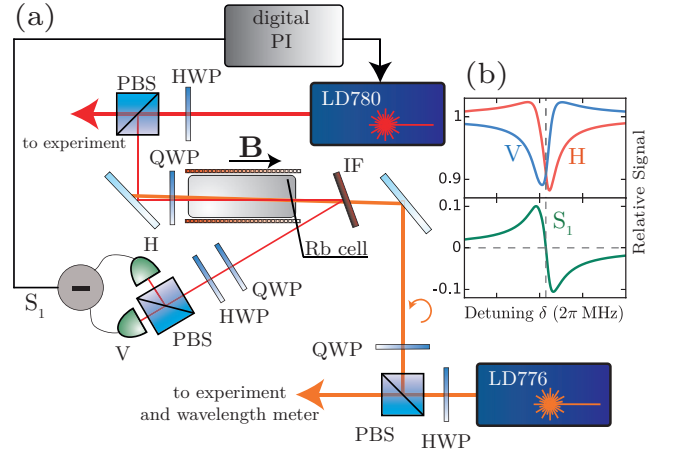


Figure 2. (a) Experimental configuration of the locking setup and (b) exemplary normalized signals H and V registered with two photodiodes of a balanced detector and the difference of the two signals S_1 demonstrating dispersive shape for magnetic field of 24 G.

the difference signal, being proportional to the normalized Stokes parameter $S_1 = (\langle E_x^2 \rangle - \langle E_y^2 \rangle) / (\langle E_x^2 \rangle + \langle E_y^2 \rangle)$ of the probe field:

$$S_1 \propto |\mathbf{A}_1|^2 (\text{Re}\chi_{1,q_2} - \text{Re}\chi_{-1,q_2}). \quad (5)$$

This expression, being the difference of real, dispersive parts of susceptibilities for two circular polarizations is also proportional to polarization rotation angle. See reference for Mathematica notebook containing implementation of the above calculations²⁵.

In our experimental implementation, we observe polarization rotation of the probe light using a polarizing beamsplitter (PBS) and a balanced detector, as shown in Fig. 2(a). Exemplary shapes of signals registered by the two photodiodes, exhibiting both dispersive and absorptive behavior, are shown in Fig. 2(b). Their difference shows purely dispersive behavior, with a steep slope in the center of resonance. To stabilize the laser frequency, we feed the locking signal to a digital proportional-integral (PI) controller, which subsequently adjusts current in the 780 nm laser diode (LD780, Toptica DL100 DFB). The 776 nm laser (LD776, Toptica DL100 ECDL) is stabilized using a commercial wavelength meter (Angstrom HighFinesse WS7), which recently proved to be very suitable for laser frequency stabilization²⁶. In the 5-cm-long rubidium vapor cell the two beams counter-propagate, having $1/e^2$ diameters of 500 μm . Maximum drive power is 50 mW, while the probe power is 500 μW . Probe light is separated using an interference filter (IF, Thorlabs FBH780-10), tilted to reflect 780 nm light and transmit 776 nm light. Additional quarter-wave plates (QWP) before and after the cell are used to compensate for the birefringence of cell windows and the interference filter. Half-wave plate (HWP) is used to adjust balance of the detector. Drive field σ_- polarization is set using a single QWP.

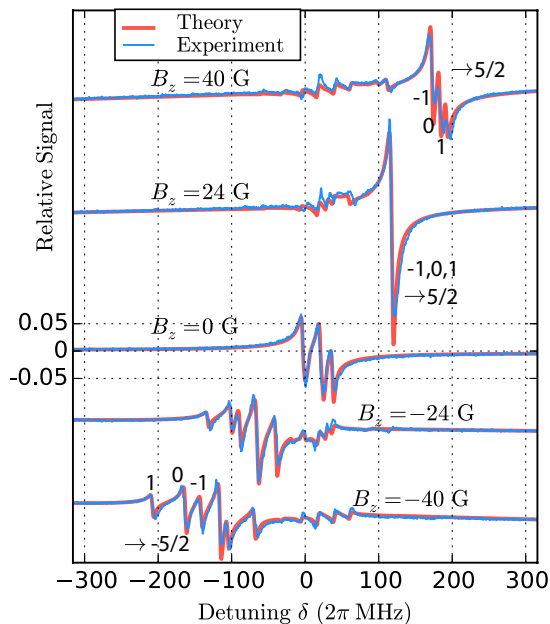


Figure 3. Exemplary locking signals normalized to sum of signals detected by two photodiodes H and V for different magnetic fields B_z , $\Delta = 2\pi \times 4$ GHz and $I_2 = 240$ mW/mm². Two-photon resonances $F = 1$; $m_F = -1, 0, 1 \rightarrow m_J = 5/2$ are marked.

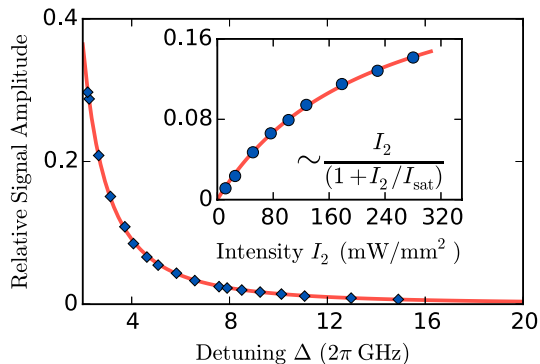


Figure 4. Locking signal peak-to-peak amplitude for $B_z = 24$ G and drive field intensity $I_2 = 240$ mW/mm² measured as a function of single-photon detuning Δ (data points) demonstrating expected inverse- Δ^2 dependance (solid line). Inset shows dependance of the signal amplitude on drive field intensity I_2 for $\Delta = 2\pi \times 3$ GHz.

For the experimental proof-of-principle demonstration we choose a transition from the ground state $5S_{1/2}, F = 1$. For the simplicity of notation from now on we measure the single-photon detuning Δ from $5S_{1/2}, F = 1$ state, just as in Fig. 1. Note that magnetic splittings of both the ground state and the intermediate state are insignificant when compared to the single-photon detuning Δ , and consequently in Eq. 3 we take $(\Delta - \omega_{0,\alpha} + \omega_{1,\alpha'})^2 \approx \Delta^2$ for each α and α' .

In the first measurement we fix the detuning of 776 nm laser and scan the detuning of 780 nm laser around

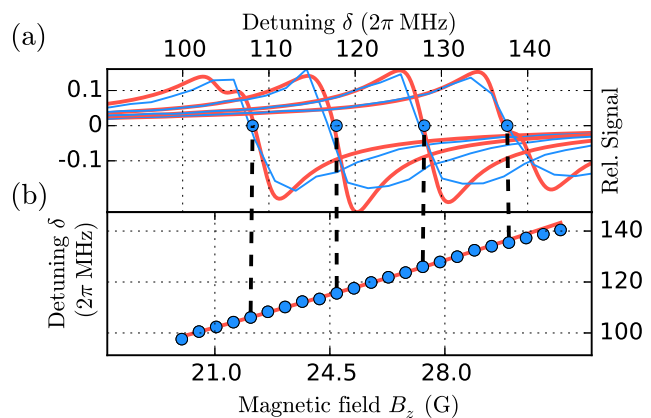


Figure 5. Tuning of the steep locking signal obtained around $B_z = 24$ G: (a) exemplary signals for $B_z = 22, 24.5, 27.3$ and 29.7 G (from left to right), (b) zero-crossing of the signal with predicted linear dependance on detuning. This line corresponds to $F = 1$; $m_F = -1, 0, 1 \rightarrow m_J = 5/2$ two-photon resonances.

the two-photon resonance. This situation corresponds to virtually constant single-photon detuning Δ and varying two-photon detuning δ . For different magnetic fields we obtained shifted signals. For magnetic fields exceeding 15 G m_J is a good quantum number describing magnetic states of $5D_{5/2}$ manifold. Consequently, lines that most rapidly shift in magnetic field correspond to highest $m_J = 5/2$, while the barely shifted lines in the middle correspond to $m_J = 1/2$ states. Splitting of the ground state only slightly influences shifting, but has significant influence on signal shape. With our theoretical model we are able to predict these shapes, and as seen in Fig. 3 we obtain excellent conformity of theoretical prediction and experimental data. The relaxation rate of highest excited state γ was adjusted for additional broadening (mainly transit-time broadening and residual Doppler broadening^{27,28}) and found to be $2\pi \times 4.2$ MHz. Finally, note that instead of changing the sign of magnetic field, one may equivalently change drive field polarization to the opposite.

Apart from the two-photon rotation, we also observed background signal from single-photon Faraday effect at $|0\rangle \rightarrow |1\rangle$ transition. This effect can easily be compensated by rotating the HWP.

At B_z around 24 G we obtain enhanced signal, corresponding to $F = 1 \rightarrow m_J = 5/2$ transitions triplet. Enhancement is due to constructive interference of contributions from different magnetic ground-state levels assisted by compensation of splittings of initial and final states. In Fig. 4 we changed the single photon detuning Δ and observed expected inverse- Δ^2 dependance (see Eq. 2). In our setup, the signal to electronic noise ratio is high enough for locking at single-photon detunings up to $\Delta = 20$ GHz, where we obtain SNR = 8. We consistently found the signal to scale linearly with probe field intensity. The signal scales linearly with the drive field

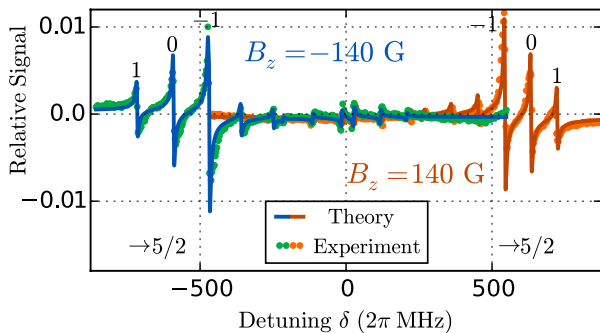


Figure 6. Calculated error signal for $I_2 = 240 \text{ mW/mm}^2$, $\Delta = 2\pi \times 8 \text{ GHz}$ and two opposite large values of magnetic field demonstrating tunability of two-photon offset frequency of over 1 GHz. Strongest marked resonances correspond to $m_F = -1, 0, 1 \rightarrow m_J = 5/2$ transitions.

intensity for higher single-photon detunings as well, but closer to resonance the signal saturates²⁸ as shown in the inset of Fig. 4.

Finally, we vary the magnetic field around 24 G and observe linear tuning of the zero-crossing of the signal. Four exemplary shapes are shown in Fig. 5(a). Linear dependance of the zero-crossing point on magnetic field is illustrated in Fig. 5(b). We found the proportionality constant to be $2\pi \times 4.06 \text{ MHz/G}$. This gives us an estimate on required stability of magnetic field. For example, for 10 kHz stability we require magnetic field instability to be lower than 3 mG, maximum drive laser power instability of 1% at 50 mW drive power and temperature instability less than 0.5°C , which are within the reach of current technical capabilities.

We envisage that higher magnetic field allows very broad tunability²⁸. Fig. 6 shows the signal calculated and measured for blue-detuning $\Delta = 2\pi \times 8 \text{ GHz}$ and $B_z = 140 \text{ G}$ and -140 G , demonstrating possibility of locking at two-photon detuning δ from $-2\pi \times 700 \text{ MHz}$ to $2\pi \times 700 \text{ MHz}$.

In conclusion, we have proposed and realized a setup enabling modulation-free tunable offset locking at a two-photon ladder transition. Tunability is achieved thanks to the splitting of the highest excited state in constant external magnetic field. Even though polarization spectroscopy is widely used, it is the first proposal of using magnetic field to tune the two-photon offset frequency. At low magnetic fields we obtain signal insusceptible to environmental perturbations. The wide range of tuning does not require any modulation. We note that configuration of fields may be easily changed in our setup, as well as in theoretical model, to use the \mathbf{A}_1 field on $|0\rangle \rightarrow |1\rangle$ transition as drive field. This would provide the feedback for laser coupled to $|1\rangle \rightarrow |2\rangle$ transition. Another method would be to simply supply the error signal as feedback to the 776 nm laser^{12,19}. The setup we demonstrated could be also used to stabilize the two-photon detuning when the excitation is done in a frequency-degenerate scheme (e.g. by 778 nm light

in case of $5S_{1/2} \rightarrow 5D_{5/2}$ transition)²⁹, possibly providing even narrower line due to perfect cancellation of Doppler-broadening, or alternatively at transitions including telecommunication wavelengths¹³.

This work has been supported by Polish Ministry of Science and Higher Education ‘‘Diamantowy Grant’’ Project No. DI2013 011943, National Science Center Grant No. DEC-2011/03/D/ST2/01941 and by the Seventh Framework Programme PhoQuS@UW Project (Grant Agreement No. 316244). We acknowledge generous support of T. Stacewicz and K. Banaszek, as well as careful proofreading of the manuscript by M. Jachura and M. Dąbrowski.

REFERENCES

- ¹T. Peyronel, O. Firstenberg, Q.-Y. Liang, S. Hofferberth, A. V. Gorshkov, T. Pohl, M. D. Lukin, and V. Vuletić, *Nature* **488**, 57 (2012).
- ²R. Drampnyan, S. Pustelny, and W. Gawlik, *Physical Review A* **80**, 033815 (2009).
- ³S. Wu, T. Plisson, R. C. Brown, W. D. Phillips, and J. V. Porto, *Physical Review Letters* **103**, 173003 (2009).
- ⁴B. Yang, Q. Liang, J. He, and J. Wang, *Optics Express* **20**, 11944 (2012).
- ⁵M. Parniak and W. Wasilewski, *Physical Review A* **91**, 023418 (2015).
- ⁶A. A. M. Akulshin, R. J. R. McLean, A. I. Sidorov, and P. Hanaford, *Optics Express* **17**, 22861 (2009).
- ⁷A. Kölle, G. Epple, H. Kübler, R. Löw, and T. Pfau, *Physical Review A* **85**, 063821 (2012).
- ⁸M. Parniak, A. Leszczyński, and W. Wasilewski, (2015), [arXiv:1512.00385](https://arxiv.org/abs/1512.00385).
- ⁹A. M. Akulshin, B. V. Hall, V. Ivannikov, A. A. Orel, and A. I. Sidorov, *Journal of Physics B: Atomic, Molecular and Optical Physics* **44**, 215401 (2011).
- ¹⁰H. S. Moon, W. K. Lee, L. Lee, and J. B. Kim, *Applied Physics Letters* **85**, 3965 (2004).
- ¹¹S. C. Bell, D. M. Heywood, J. D. White, J. D. Close, and R. E. Scholten, *Applied Physics Letters* **90**, 171120 (2007).
- ¹²R. P. Abel, A. K. Mohapatra, M. G. Bason, J. D. Pritchard, K. J. Weatherill, U. Raitzsch, and C. S. Adams, *Applied Physics Letters* **94**, 071107 (2009).
- ¹³Y. N. Martinez de Escobar, S. Palacios Álvarez, S. Coop, T. Vanderbruggen, K. T. Kaczmarek, and M. W. Mitchell, *Optics Letters* **40**, 4731 (2015).
- ¹⁴C. Wieman and T. W. Hänsch, *Physical Review Letters* **36**, 1170 (1976).
- ¹⁵H.-R. Noh, *Optics Express* **20**, 21784 (2012).
- ¹⁶P. F. Liao and G. C. Bjorklund, *Physical Review Letters* **36**, 584 (1976).
- ¹⁷R. Hamid, M. Çetintaş, and M. Çelik, *Optics Communications* **224**, 247 (2003).
- ¹⁸B. Yang, J. Wang, H. Liu, J. He, and J. Wang, *Optics Communications* **319**, 174 (2014).
- ¹⁹F. E. Becerra, R. T. Willis, S. L. Rolston, and L. A. Orozco, *Journal of the Optical Society of America B* **26**, 1315 (2009).
- ²⁰M. Dąbrowski, R. Chrapkiewicz, and W. Wasilewski, *Journal of Modern Optics* (2015), [10.1080/09500340.2015.1106016](https://doi.org/10.1080/09500340.2015.1106016).
- ²¹J. A. Zielńska, F. A. Beduini, N. Godbout, and M. W. Mitchell, *Optics Letters* **37**, 524 (2012).
- ²²C. Tai, W. Happer, and R. Gupta, *Physical Review A* **12**, 736 (1975).
- ²³D. A. Steck, ‘‘Rubidium 87 D line data,’’ (2001).
- ²⁴D. Sheng, A. Pérez Galván, and L. A. Orozco, *Physical Review A* **78**, 062506 (2008).

- ²⁵M. Parniak, A. Leszczyński, and W. Wasilewski, “Mathematica Notebook for: Magneto-optical polarization rotation in a ladder-type atomic system for tunable offset locking,” 10.6084/m9.figshare.2067036.
- ²⁶K. Saleh, J. Millo, A. Didier, Y. Kersalé, and C. Lacroûte, *Applied Optics* **54**, 9446 (2015).
- ²⁷H. S. Moon and H.-R. Noh, *Journal of the Optical Society of America B* **31**, 1217 (2014).
- ²⁸See supplemental material at ftp://ftp.aip.org/epaps/appl_phys_lett/E-APPLAB-108-027616/SupplementaryMaterial.pdf for further discussion of saturation effects, line broadening and tuning at high magnetic fields.
- ²⁹E. Brekke and E. Herman, *Optics Letters* **40**, 5674 (2015).